American Mineralogist, Volume 82, pages 109–124, 1997

Corrensite: A single phase or a mixed-layer phyllosilicate in the saponite-to-chlorite conversion series? A case study of Sancerre-Couy deep drill hole (France)

DANIEL BEAUFORT,[1] ALAIN BARONNET,[2] BRUNO LANSON,[3] AND ALAIN MEUNIER[1]

[1]URA 721 CNRS, Université de Poitiers 40 Ave. du Recteur Pineau, 86022 Poitiers cédex, France
[2]Centre de Recherche sur les Mécanismes de la Croissance Cristalline (CRMC²), CNRS, Campus Luminy, Case 913, 13288 Marseille cédex 9, France
[3]LGIT IRIGM, Environmental Geochemistry Group, University J. Fourier, CNRS, BP 53X, 38041 Grenoble cédex, France

ABSTRACT

Transmission electron microscopy (TEM), analytical electron microscopy (AEM), and decomposition-simulation of X-ray diffraction (XRD) patterns were used to characterize trioctahedral clay from Sancerre-Couy that had previously been considered to be a mixed-layer material of chlorite-smectite (C-S). Corrensite should not be regarded as a regular, 50:50 mixture of chlorite and smectite mixed layers but as a true phase in the thermodynamic sense with a discrete stability field and paragenetic relationships with saponite and chlorite. C-S was not found to exist; the clay is composed of saponite or mixtures of corrensite, chlorite, and minor amounts of chlorite-corrensite mixed layers (C-C). Corrensite layers from different samples have a constant AEM composition (except for Fe/Mg ratio). The *b* parameter of corrensite is not compatible with a simple association of chlorite and smectite layers. Chlorite-like and smectite-like sublayers of corrensite do not behave independently during crystal growth. Selected-area electron diffraction (SAED) patterns and decomposition of XRD profiles provide evidence of C-C mixed layers. The conversion of corrensite to chlorite occurred by two simultaneous processes: (1) intergrowth of coherently stacked layers of chlorite leading to a mixture of discrete chlorite and corrensite crystallites; and (2) chlorite-corrensite random mixed layering in the case of very intimate associations of chlorite and corrensite domains. Intergrowths largely predominate over mixed layers because the solubility between corrensite and chlorite layers is low. These C-C mixed layers cannot be considered as interstratified minerals sensu stricto as may be the case for the smectite-to-illite conversion series.

INTRODUCTION

Corrensite is well known as the trioctahedral variety of regular, 50:50 mixed-layer chlorite-smectite and chlorite-vermiculite. Its original definition was proposed by Lippmann (1956) and has been recognized by the Nomenclature Committee of the Clay Mineral Society (Bailey 1982). It is by far the dominant type of mixed-layer chloritic mineral encountered in natural systems (Reynolds 1988). Occurrences of corrensite are numerous in environments with low to moderately elevated temperatures. It has been reported in saline deposits and evaporites (Bodine and Madsen 1987), sedimentary rocks (April 1981a, 1981b), weathering (Johnson 1964; Post and Janke 1974), volcanic and sedimentary sequences (Schultz 1963; Whitney and Northrop 1986), burial diagenesis (Hoffman and Hower 1979; Chang et al. 1986), fossil and active hydrothermal systems (Kristmannsdottir 1979; Beaufort and Meunier 1983, 1994; Inoue 1987; Bettison and Schiffman 1988; Inoue and Utada 1991; Meunier et al. 1991), contact-metamorphic aureoles (April 1980; Vergo and April 1982), and low-grade regional metamorphism (Shau et al. 1990).

In all these occurrences, the structural and thermodynamic nature of corrensite needs further clarification. Indeed, several of the papers cited above were concerned with corrensite phase relations. Should corrensite be considered as a regular mixed-layer structure that belongs to a continuous conversion series from swelling trioctahedral phyllosilicates (smectite or vermiculite) to chlorite? Or should it be considered as a single mineral that consists of a regular alternation of chlorite and swelling trioctahedral phyllosilicate, giving a rational X-ray diffraction (XRD) pattern? We note that chlorite can be viewed as a regular alternation of talc and brucite layers, but it is still considered a single mineral. In the case of a single mineral, corrensite is a phase in the thermodynamic sense, with a discrete stability field and definable phase relations with smectite, vermiculite, and chlorite (Velde 1977; Shau et al. 1990). Consequently, the clay minerals reported as chlorite-smectite with >50% chlorite layers would have to be reinterpreted as a physical mixture or interstratification of corrensite and chlorite elementary layers rather than as interstratified chlorite-smectite or chlorite-vermiculite. Reynolds (1988) explained that, ex-

0003–004X/97/0102–0109$05.00

cept for very favorable cases, XRD studies alone are insufficient to identify the ordering type of chlorite-smectite minerals (C-S) that deviate, even slightly, from the 50:50 ratio because of a dramatic reduction in the intensity of the large interplanar spacing.

In the present study, we investigated the chemistry and microstructure of various trioctahedral phyllosilicate minerals encountered in the metamorphic basement of the Sancerre-Couy deep drill hole. This chloritic material includes saponite, corrensite, and a series of trioctahedral phyllosilicates that ranges compositionally from corrensite to nearly pure chlorite. This material appears to be a good candidate for evaluation of the "single phase" hypothesis for corrensite. Microchemical analyses of clay veins by electron microprobe analysis (EMPA), XRD, scanning electron microscopy (SEM), and high-resolution transmission electron microscopy (HRTEM), coupled with analytical electron microscopy (AEM), were used to investigate the phase relations between corrensite, saponite, and chlorite from the scale of millimeters to nanometers (individual layer).

In this study the distinction between a chlorite-saponite mixed-layer series and an assemblage of saponite, corrensite, and chlorite phases is made on the basis of the following criteria. (1) A constant morphology across the compositional series would suggest simple mixing of C-S across the compositional join, whereas a distinct morphology for corrensite suggests a distinct crystalline material. (2) TEM observations of regular interstratification and coexisting regular interstratifications of given layer types, with constant composition, and with discrete chlorite or saponite, indicate a primary phase stability for corrensite. (3) Simulation of XRD patterns, as constrained by TEM observations, indicates whether C-S or chlorite-corrensite mixed layers (C-C) are found in samples.

Materials and methods

Geologic setting

The metamorphic basement (380 Ma) of the southern part of the Paris Basin was drilled at Sancerre-Couy (scientific drilling, Programme de Géologie Profonde de la France). This basement is composed of hornblende + clinopyroxene + garnet amphibolites alternating with biotite + garnet gneisses. These metamorphic units experienced a retrograde episode during which small amounts of chlorite + epidote or chlorite + phengite assemblages crystallized. A NNE-SSW distensive tectonic phase at the end of the Hercynian orogenesis produced fractures that were subsequently sealed by multistage mineral deposits. Trioctahedral clay minerals represent the last crystallization episode within the fracture network (Beaufort et al. 1991). The nature of these trioctahedral clay minerals varies as a function of the host-rock chemistry and is independent of depth. Corrensite is the most common clay mineral; it is especially abundant in fractured amphibolite and mafic gneiss. Saponite occurrences are restricted to a few units of pyroxene-rich amphibolite, whereas chloritic mixed-layer minerals (>50% chlorite) are common in gneiss.

The crystallization of clay minerals within fractures is associated with a thin halo of wall-rock alteration in which mafic silicates (pyroxene, hornblende, biotite, and chlorite), as well as feldspar and calcite of metamorphic and earlier hydrothermal episodes, have been destabilized. The study of the fluids presently trapped in these fractures (Boulègue et al. 1990; Boulègue and Megnien 1992) and the isotopic data (C, O) of various infilling silicates and carbonates (Fouillac and Beaufort 1991, 1992) indicate that the trioctahedral clays precipitated over a very long period in response to the interaction of very saline sedimentary or hydrothermal fluids (brines?), previously trapped in the fracture network, with mafic minerals of the host rocks. Alteration of the wall rock was limited because solutions were not renewed.

Previous work

The chemistry of trioctahedral clay minerals from Sancerre-Couy was investigated by Beaufort and Meunier (1994) and may be summarized as follows: (1) Saponite, corrensite, and chloritic mixed layers with chlorite contents ranging from 50 to 90% (on the basis of equivalent chlorite to smectite ratio) were observed by XRD and EMPA performed on 62 separates of clay material from veins. (2) Mixed-layer minerals with compositions intermediate between saponite and corrensite were not observed. (3) The statistical distribution of Si, Al, and Mg established by EMPA indicates bimodal chemical populations in corrensite and chloritic mixed layers and suggests a mixture of two types of particles. (4) The octahedral sites of saponite and chlorite, which are supposed to be interstratified in these trioctahedral phyllosilicates, seem to be completely filled. (5) The expandable layer of corrensite deduced from structural formulas normalized to 50 O atoms has a rather high layer charge (mean value = 1.04).

On the basis of this previous work, we selected for further investigation four samples representing a characteristic compositional range of trioctahedral clay minerals at Sancerre-Couy: a sample containing pure saponite (SC1001), a sample containing nearly pure corrensite (SC1603), and two samples of chloritic mixed layers containing 75% (SC1379) and up to 90% chlorite layers (SC961).

EMPA analyses of saponite, corrensite, and chlorite mixed layers of the selected samples differentiate swelling trioctahedral phyllosilicates with low- and high-charge expandable layers (Table 1; Fig. 1). Microchemical analyses are not useful in the investigation of the nature of the interlayered species (saponite or corrensite) in the chloritic material. However, analyses of corrensite and chlorite mixed layers are scattered along a continuous line joining pure, intermediate to high layer charge corrensite with a chloritic mixed layer containing up to 90% chlorite (near the clinochlore end-member).

TABLE 1. Mean cation contents from microprobe analyses of saponite, corrensite, and chloritic mixed layers from the Sancerre-Couy deep drill hole

	SC1001*	SC1603**	SC1379†	SC961‡
Si	6.91	12.90	12.06	6.35
Al	1.25	5.35	6.08	3.83
Fe^{2+}§	1.16	4.47	6.17	2.37
Mg	4.72	11.22	10.27	7.10
Ti	0.00	0.01	0.01	0.01
Mn	0.01	0.07	0.03	0.01
Ca	0.28	0.34	0.25	0.06
Na	0.12	0.05	0.02	0.02
K	0.13	0.05	0.03	0.02
Int. Ch.	0.81	0.78	0.55	0.16
Oct.	6.06	18.02	18.62	11.66
Fe/(Fe + Mg)	0.20	0.28	0.38	0.25
Se/(Si + Al)	0.85	0.71	0.66	0.62

* 171 analyses normalized to 22 O atoms.
** 299 analyses normalized to 50 O atoms.
† 38 analyses normalized to 50 O atoms.
‡ 116 analyses normalized to 28 O atoms.
§ All Fe as Fe^{2+}.

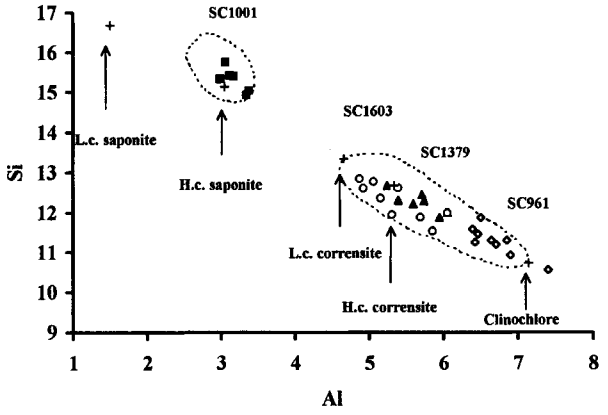

FIGURE 1. Si vs. total Al for samples SC1001, SC1603, SC1379, and SC961 on the basis of $O_{40}(OH)_{20}$. The compositions of ideal low-charge (L.c.) and high-charge (H.c.) saponite and corrensite, as well as the composition of clinochlore, are given for reference. Dashed regions correspond to EMPA data, and symbols correspond to AEM data.

Experimental methods

Clay material observed in thin sections was extracted by microdrilling and separated and purified by sedimentation and ultracentrifugation. XRD was performed with a Philips PW 1729 diffractometer (40 kV, 40 mA) equipped with a SOCABIM system for numerical data acquisition. The XRD system used Ni-filtered Cu$K\alpha_{1,2}$ radiation, a soller slit on the incident beam, and a graphite monochromator. The divergence slit, scatter slit, and receiving slit were, respectively, 1°, 0.1 mm, and 1°. The usual step size and counting times were, respectively, 0.01° 2θ and 10 s for both air-dried and ethylene glycol-saturated samples. The characteristics of the superimposed XRD reflections (position, intensity, and FWHM) were determined by decomposition of diffractograms using the DECOMPXR program (Lanson and Besson 1992). Amounts of expandable layers were determined by comparison with XRD patterns calculated with the program NEWMOD (Reynolds 1985).

Microchemical analyses of clay minerals were obtained with a CAMECA SX50 microprobe using wavelength-dispersive spectrometry. Analytical conditions were as follows: 15 kV, 4 nA, 10 s counting time, and a 1 μm spot size. The system was calibrated using synthetic and natural oxides and silicates. Corrections were made with a ZAF program. The reproducibility of standard analyses is ±1%. At least 30 analyses were performed at each location.

SEM observations were made using a JEOL 6400 instrument on small, freshly fractured core samples that were coated with gold. TEM and AEM analyses were made on microdrilled disks centered on phyllosilicate-rich zones from selected thin sections. Standard single-hole copper grids were glued on the disks, and the disk-grid assemblies were detached from the glass slide substrate by gentle, local heating. Repeated washing in absolute ethanol removed excess Lakeside resin prior to ion thinning with a Gatan 600 Duomill machine (5 kV, 0.25 mA per gun, 20°, and finish angle of 150) working at room temperature. A thin (150–200 Å) carbon coating completed the sample preparation.

TEM and AEM analyses were performed with the CRMC² JEOL 2000 FX electron microscope working at 200 kV. The microscope is equipped with a Tracor TN-5502 system for energy-dispersive microanalysis. Lattice-fringe images were obtained by short, through-focus series of micrographs bracketed from −600 to −1200 Å defocus (Scherzer focus is −950 Å) using mostly 00*l* diffracted beams and the *hh* and 02*k* weak and diffuse reflections that passed through a 0.36 $Å^{-1}$ objective aperture. In this paper *hk* refers to two-symbol Miller indices of diffraction rods, which represent Fourier transforms of single layers or of thin semicoherent packets of layers. The Lhesa low-light camera used to optimize imaging conditions greatly improved the final quality of high-resolution images taken at low direct magnification (150000×) by decreasing beam damage. As recommended by Guthrie and Veblen (1990), we used intermittent strong objective overfocusing to reveal mixed layer ordering from both chemically and structurally enhanced contrasts of basal lattice fringes. Selected-area electron diffraction patterns (SAED) were recorded with an aperture selecting 4000 Å in the object plane.

AEM was performed in fixed-electron–beam mode (200–400 Å beam diameter, 1.2 nA beam current, 100s counting time) after removing the objective aperture. After confirming that electron channeling had minor analytical effects (Baronnet et al. 1993), data were collected without tilting the specimen away from the orientation used for high-resolution imaging. No absorption correction was necessary because of the high (72°) take-off angle for collected X-rays. Raw data were processed by the SMTF program (Cliff and Lorimer 1975). The $k_{x,Si}$ factors

were experimentally calibrated against synthetic and natural layer silicates for x = Mg, Al, Fe, and K, whereas built-in factors were used for x = Ca and Na. Microchemical data were collected in thin zones that were structurally continuous with those imaged by HRTEM.

Results

Sample SC1001 (saponite)

XRD patterns of the saponite sample (SC1001) in air-dried (AD) and ethylene glycol–saturated states (EG) are typical of a clay material composed of 100% smectite layers, with a very low saddle/001 peak ratio in both diffractograms (Fig. 2). Nevertheless, these expandable layers are probably not homogeneous. The 001 reflection position (16.95 Å) and the very low intensities of other 00*l* reflections observed on the EG pattern have been satisfactorily simulated by mixing equal proportions of low- and high-charge trioctahedral smectite (saponite) (Beaufort and Meunier 1994).

The saponite sample observed by SEM appears as highly folded thin films of anhedral crystals organized in honeycomb arrangements perpendicular to the edges of fractures (Fig. 3a). Observed by TEM, saponite presents intergrown aggregates of packets typically 10–100 layers in thickness. These packets are often slightly misoriented with respect to each other (subgrain to low-angle grain boundaries). Within each packet, single layers are collapsed to 10 Å and in some places have limited lateral extent (Fig. 4), thus forming edge dislocation-like features among (00*l*) lattice-fringe patterns. HRTEM does not show any evidence of interlayering resulting from the insertion of structurally or chemically different layers.

SAED patterns with the electron beam along any direction parallel to the layers are similar and exhibit rather patchy 00*l* spots and pairs of 02,11 and 20,13 diffraction arcs bracketing the 00*l* rows at distances of approximately (4.5 Å)$^{-1}$ and (2.6 Å)$^{-1}$, respectively. [Here, the notation (4.5 Å)$^{-1}$ represents the reciprocal distance, or $\frac{1}{4.5}$ Å (0.222 Å^{-1}).] The blurry 00*l* reflections may be accounted for both by incomplete collapse and by ubiquitous curvature of the layers. The layer collapse is clearly indicated by lenticular cleavage openings that are more numerous and better developed close to the ion-thinned wedge (Fig. 4). SAED patterns taken normal to the layers display continuous *hk* diffraction rings even in thin regions. This observation indicates predominant turbostratic stacking, i.e., the stacking of consecutive layers is characterized by rotational as well as translational disorder.

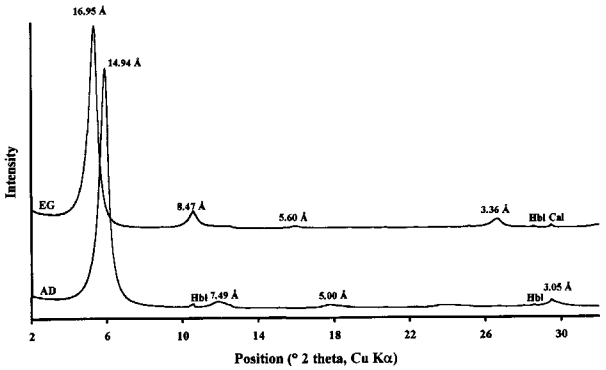

FIGURE 2. XRD patterns of saponite (SC1001), air dried (AD) and after ethylene glycol solvation (EG). Hbl = hornblende, Cal = calcite.

AEM chemical analyses of saponite are consistent with saponite (i.e., the interlayer charge essentially compensates the tetrahedral substitution of Al for Si; Fig. 1 and Table 2). In comparison with the mean microprobe analysis (Table 1), the analyses differ only by a higher interlayer charge. Heterogeneous interlayer charge of this smectitic material was observed previously (Beaufort and Meunier 1994).

Sample SC1603 (corrensite)

XRD patterns of sample SC1603 (Figs. 5 and 6) are typical of the corrensite structure with sharp superstruc-

TABLE 2. Representative AEM analyses from 200 to 400 Å packets containing saponite layers only (SC1001), mainly corrensite layers [SC1603-1 and SC1379-1] and a mixture of chlorite + corrensite layers (SC1379-2 and SC961)

	SC1001*	SC1603-1**	SC1603-2**	SC1379-1**	SC1379-2**	SC961†
Si	6.75	12.83	11.89	12.84	11.97	6.12
Al	1.31	4.88	5.69	5.32	6.00	3.86
Fe^{2+}	1.14	4.20	4.62	5.92	6.41	2.83
Mg	4.83	12.23	12.77	10.06	10.34	7.06
Mn	n.d.	0.00	0.10	0.05	0.02	n.d.
Ca	0.21	0.46	0.10	0.39	0.18	0.05
K	0.19	0.06	0.06	0.37	0.11	0.04
Na	0.53	0.20	0.14	0.16	0.15	0.00
Int. Ch.	1.14	1.18	0.40	1.31	0.62	0.14
Oct.	6.02	18.14	19.07	18.20	18.73	11.88
Fe/(Fe + Mg)	0.19	0.26	0.27	0.37	0.38	0.29
Si-Si + Al	0.84	0.72	0.68	0.71	0.67	0.60

* Normalized to 22 O atoms.
** Normalized to 50 O atoms.
† Normalized to 28 O atoms.
‡ All Fe as Fe^{2+}.

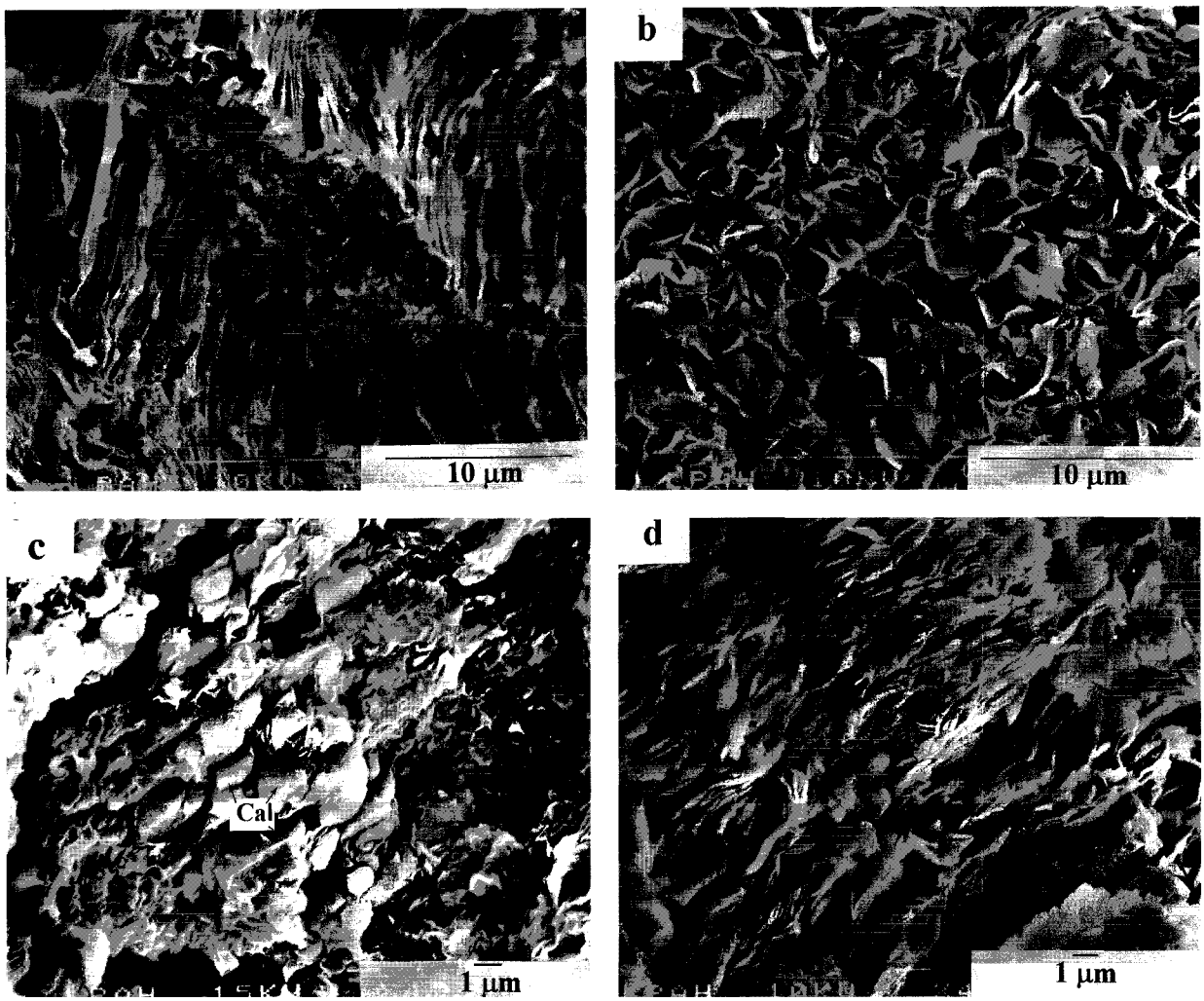

FIGURE 3. Scanning electron microphotographs of the trioctahedral mixed-layer minerals from the Sancerre-Couy deep drill hole. (**a**) Saponite from sample SC1001 appears as highly folded thin films of anhedral crystals organized in honeycomb arrangements perpendicular to the edges of fractures. (**b**) Corrensite from sample SC1603 shows a boxwork pattern oriented perpendicular to the wall-rock surface. (**c**) Chloritic material from sample SC1379 occurs as packets of small crystals in which a boxwork pattern and oriented individual crystals are intimately associated. Cal = calcite rhombs. (**d**) Chloritic material from sample SC961 occurs as coarse packets of small (<1 μm), oriented individual crystals. The basal crystal faces typically present euhedral morphologies (black arrows).

ture reflections at 29 Å (AD) and 31 Å (EG) with 10 and 11 harmonic reflections in the 2–32° 2θ Cu$K\alpha$ range for AD and EG conditions, respectively. The sharpness of these reflections is characteristic of rather thick crystallites (the best NEWMOD simulation of this mineral was obtained with $7 \leq N \leq 20$) and is consistent with the unusually large size of the phyllosilicate flakes observed in thin section (up to several tens of micrometers). In addition to corrensite, traces of discrete chlorite were identified. It is unclear if they represent relics of dissolved metamorphic chlorites (locally observed in thin section) or discrete authigenic chlorite associated with corrensite growth.

Corrensite observed by SEM shows a boxwork pattern (Fig. 3b) oriented perpendicular to the wall-rock surface. At higher magnification the boxwork appears to be composed of packets of numerous, very thin individual crystals lying with their basal crystal faces in contact. Locally, stacked individual crystals of corrensite present euhedral shapes.

Observed at low magnification with TEM, the corrensite appears as rosettes made of curved crystals immersed in a calcite matrix. The 00*l* lattice images (Fig. 7) show a unique kind of material with 24 Å periodicity. This periodicity frequently extends over several tens of layers. The essential lack of layer-stacking error is remarkable

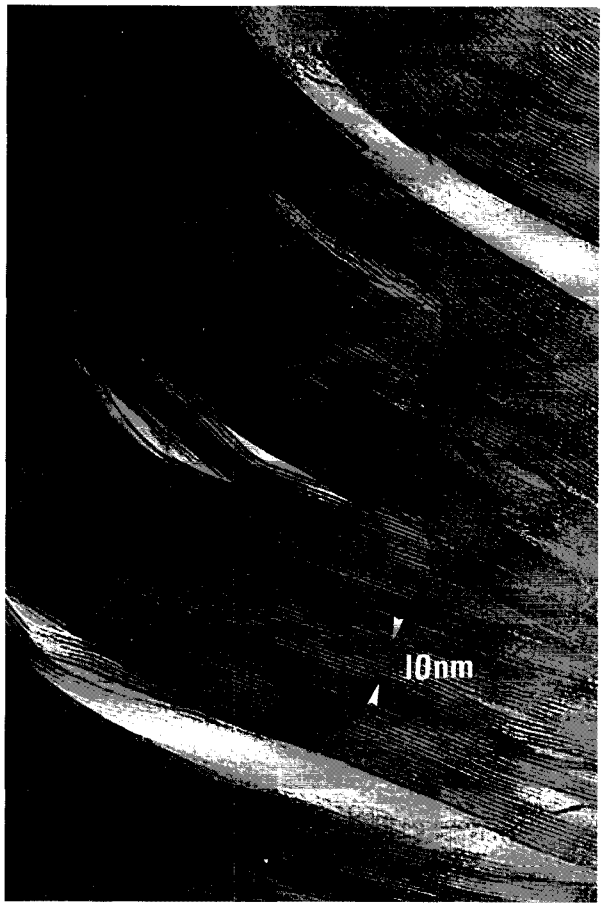

FIGURE 4. Saponite from sample SC1001. A (001) lattice image of 100% smectite material composed of bent subgrains. The single layers collapsed to ~10 Å in the vacuum. Note the total absence of layers with different thicknesses.

even where subgrain boundaries vanish, leaving parallel grains. This observation is consistent with indissociable corrensite sublayers. Within each 24 Å period, the lattice fringes delimit two (14 and 10 Å) or three (9.5, 5, and 9.5 Å) subspacings at Scherzer defocus, the relative development of which varies with the defocus of the objective lens and layer tilt (Fig. 8). Of the three subspacings, the former two may be attributed to the talc-like and brucite-like sheets of chlorite, whereas the latter may be related to collapsed smectite. This complies with previous imaging of ordered R = 1 (Reichweite) chlorite-smectite (Klimentidis and Mackinnon 1986; Vali and Koster 1986; Shau et al. 1990).

Layers always end laterally (low-angle grain boundary or edge-dislocation line; Fig. 7) in the form of a full corrensite layer or an integral multiple of it. Interruption of the regular chlorite-smectite stacking sequence (where it occurs) consists of two to three consecutive 14 Å (chlorite) layers (Fig. 8a) without any extra smectite layers, as already reported by Shau et al. (1990). SAED patterns taken along the layers (Fig. 9a) confirm the $(24\ Å)^{-1}$ periodicity along 00*l* and again display the simultaneous presence of 02,11 and 20,13 diffraction rows for any azimuthal orientation of the electron beam along the layers. This cylindrical symmetry of the diffraction pattern does indicate some turbostratic component in the layer stacking. However, the unequal distribution of intensity along *hkl* with a $(24\ Å)^{-1}$ spacing of maxima along 02*l* and 11*l* denotes some trend toward a local one-layer stacking sequence of corrensite-like layers. These two conflicting observations may be reconciled by looking at SAED patterns recorded with the electron beam normal to the layers (Fig. 9b). In this orientation, the *hk*0 diffraction rings appear spotty with unequal distances and intensities of con-

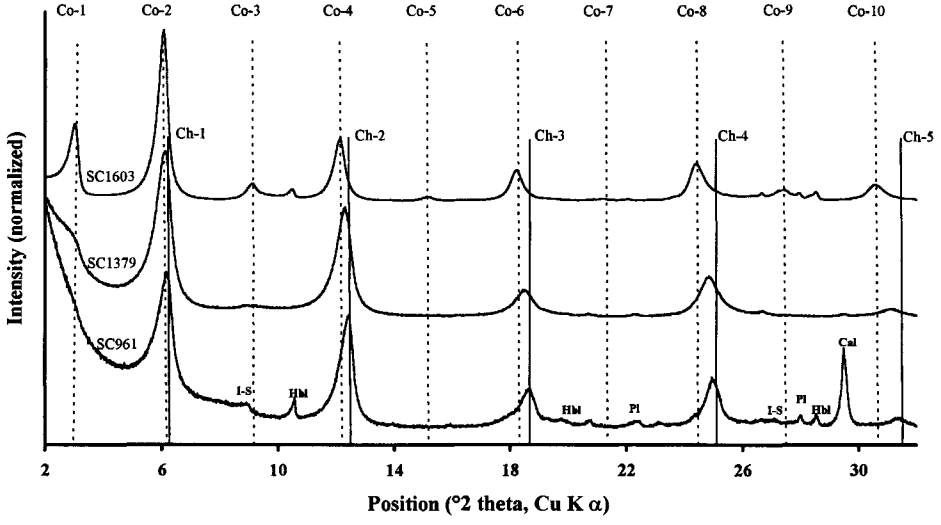

FIGURE 5. XRD patterns of air-dried corrensite (SC1603) and mixed-layer chlorite minerals with chlorite >50% (SC1379 and SC961) that were encountered in the Sancerre-Couy deep drill hole. Dashed lines depict the 00*l* peaks of the corrensite diffraction pattern, and solid lines show the positions of the chlorite reflections. Hbl = hornblende, I-S = illite-smectite mixed layer, Cal = calcite, Pl = plagioclase.

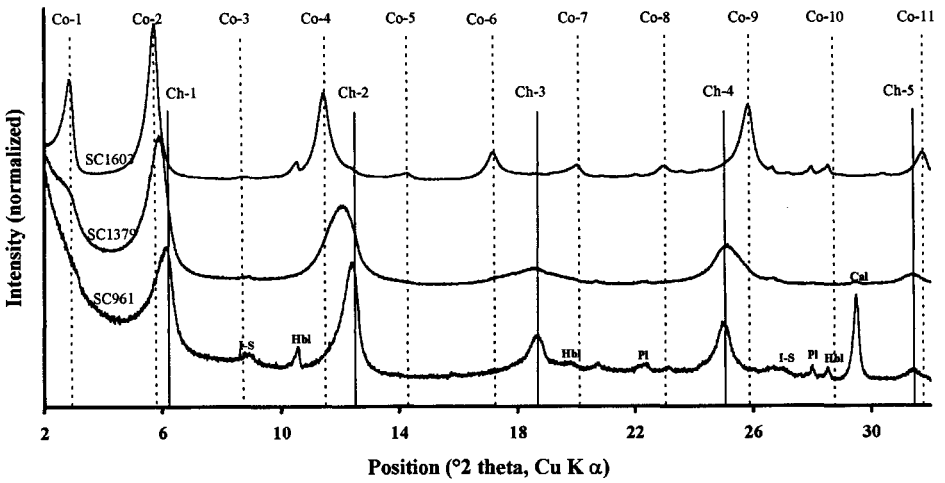

FIGURE 6. XRD patterns of ethylene glycol–saturated corrensite (SC1603) and mixed-layer chlorite minerals with chlorite >50% (SC1379 and SC961) that were encountered in the Sancerre-Couy deep drill hole. Description and abbreviations as in Figure 5.

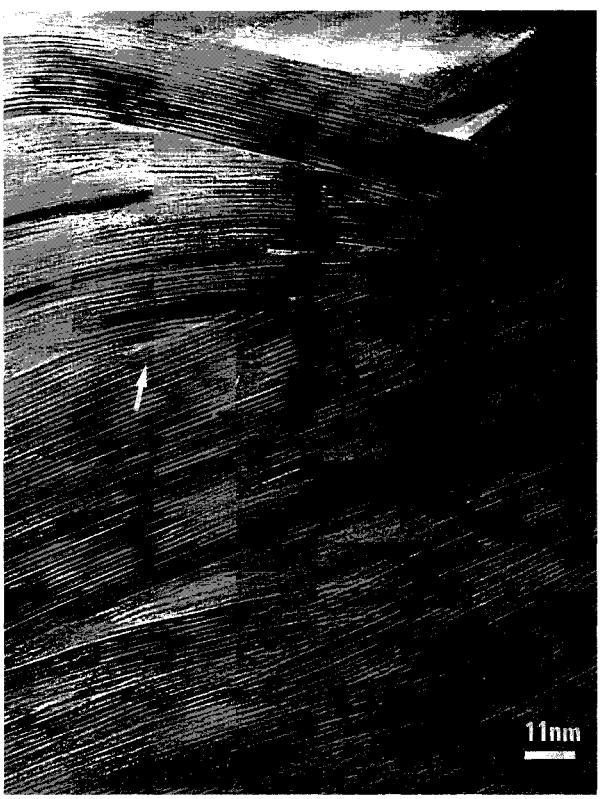

FIGURE 7. Corrensite from sample SC1603. Rosettes of corrensite crystals seen in cross section by TEM. Corrensite crystallites join as low-angle grain boundaries and edge-dislocation-like defects (white arrow). The image of the corrensite structure (e.g., upper middle and lower right) appears as a regular succession of white ~10 Å (collapsed smectite) and ~14 Å (chlorite) fringe spacings.

secutive spots. This strongly suggests that coherent domains (layers stacked with $k \cdot 60°$ or $k \cdot 120°$ rotation) of different thickness pile up turbostratically, i.e., they are linked to each other by irrational stacking angles. Where two-dimensional images are made by the combination of 02*l* and 11*l* reflections with 00*l* reflections, the thickness of those coherent slabs may vary from one (24 Å) to six (144 Å) corrensite layers (Fig. 8a).

The AEM chemical analysis of nearly pure corrensite (SC1603-1) is consistent with microprobe results, except that K and Na are much higher in the AEM analyses (Fig. 1; Table 2). This finding is consistent with the high charge characteristic of the expandable layer of corrensite. The AEM analysis of packets in which corrensite layers are intergrown with extra 14 Å (chlorite) layers (SC1603-2) differs from AEM analyses of nearly pure corrensite by having a lower Si/(Si + Al) ratio (0.68 vs. 0.72), a lower interlayer charge (0.40 vs. 1.18), and a higher octahedral occupancy (19.07 vs. 18.14). These differences are consistent with an increasing proportion of chloritic layers. The Fe/(Fe + Mg) ratio does not vary significantly between nearly pure corrensite and packets of corrensite intergrown with extra 14 Å (chlorite) layers.

Sample SC1379 (chloritic mixed layer with 75% chlorite)

XRD patterns of sample SC1379 (Figs. 5 and 6) show weak and broad superstructure reflections near 29 Å (AD) and 31 Å (EG). However, other 00*l* reflections are irrational and suggest interstratification. Peak broadening and peak asymmetry vary significantly from AD to EG patterns.

Basically, we observed that 00*l* peak broadening for sample SC1379 increases with the distance between the proximal reflections of chlorite and corrensite. This is particularly visible for peaks close to the chlorite 002 and 003 reflections (Figs. 5 and 6), and, as a consequence,

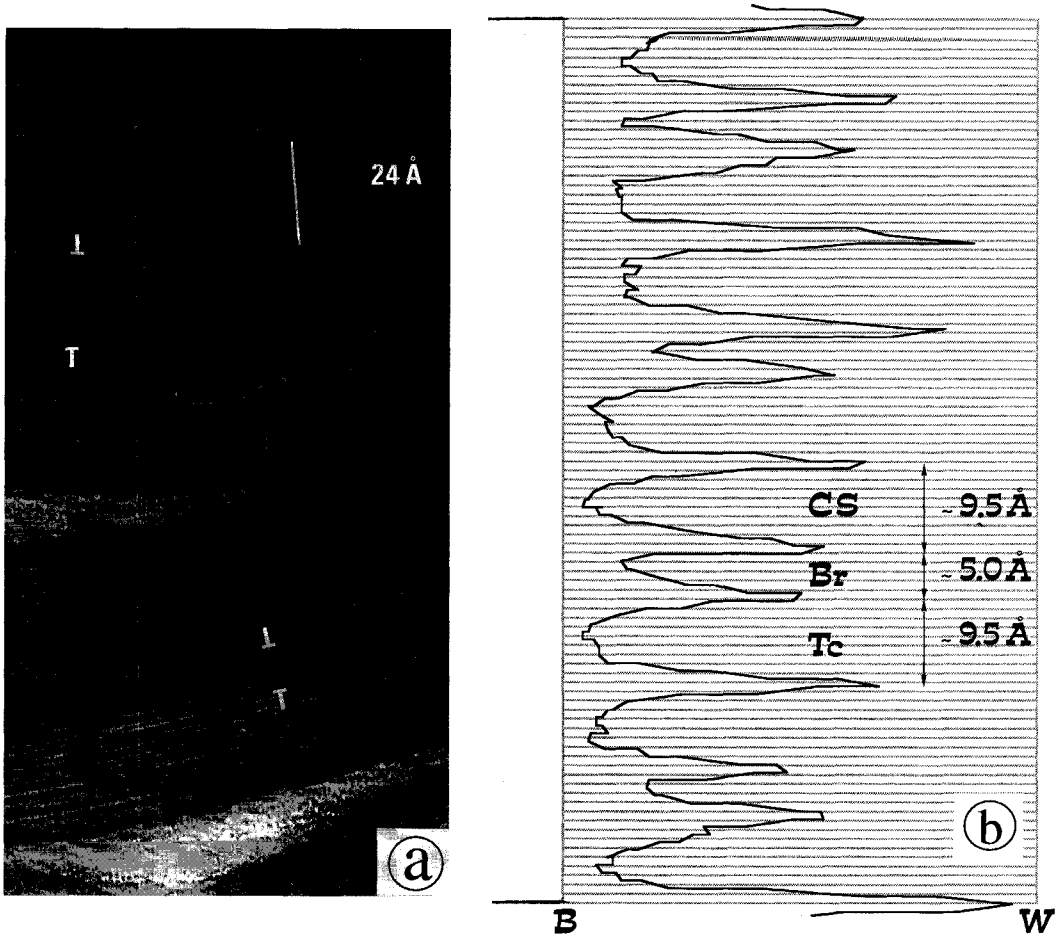

FIGURE 8. Sample SC1603. (**a**) High-resolution TEM image of corrensite slabs viewed along the layers revealing the successive talc-like + brucite-like + collapsed smectite-like sublayer. The black arrow points to a piling-up fault, which may be interpreted as one missing smectite-like layer in the regular R = 1 sequence, leaving two chlorite layers in close contact. The two T brackets enclose two-dimensionally imaged subslabs of corrensite crystals (white spotty images made by recombination of 00*l* reflections with 02*l* and 11*l* reflections). The bars of the T brackets mark transitions between two-dimensional and one-dimensional lattice images. (**b**) Intensity profile along the white bar at the top of **a**. B = black, W = white; grid bars are 1 Å apart. The collapsed corrensite repeat distance was arbitrarily calibrated at 24.0 Å. CS = collapsed smectite-like layer, Br = brucite-like layer, and Tc = talc-like layer.

the peak asymmetry observed in XRD patterns cannot be attributed to an instrumental effect. The best illustration of the above remark is given by the behavior of the peak near the chlorite 003 reflection after ethylene glycol solvation; this peak strongly broadens but remains almost symmetrical (corrensite 006 and 007 reflections are located at equal distances from the chlorite 003 reflection).

The chloritic material of sample SC1379 (Fig. 3c) shows morphological characteristics intermediate between those of samples SC1603 (Fig. 3b) and SC961 (Fig. 3d). It is composed of packets of small crystals in which structural arrangements previously described for samples SC1603 (boxwork pattern) and SC961 (oriented individual crystals) seem to be intimately associated.

The slightly misoriented crystallites of sample SC1379 have contact planes of (00*l*) against vicinal surfaces close to (00*l*) and delineate a markedly oriented texture as observed by TEM. Chlorite (and chlorite-like) and collapsed smectite-like layers image as 14 and 9–10 Å fringes, respectively (Fig. 10). This matrix is moderately defective in the form of irregularly intergrown 9–10 Å thick layers (collapsed smectite?). Because 9–10 Å thick single layers are never contiguous, they may each presumably be considered as systematically associated with a chlorite-like layer, thus forming intergrown corrensite layers into chlorite. In Figure 10 the upper white arrow also marks a transition zone from one-dimensional to two-dimensional imaging, i.e., the location of an incoherent stacking surface. Note the strong diffraction contrast change there, i.e., the strong intensity loss of the two-dimensional imaged zone in bright-field mode caused by non-00*l* reflections stopped by the objective aperture. SAED patterns

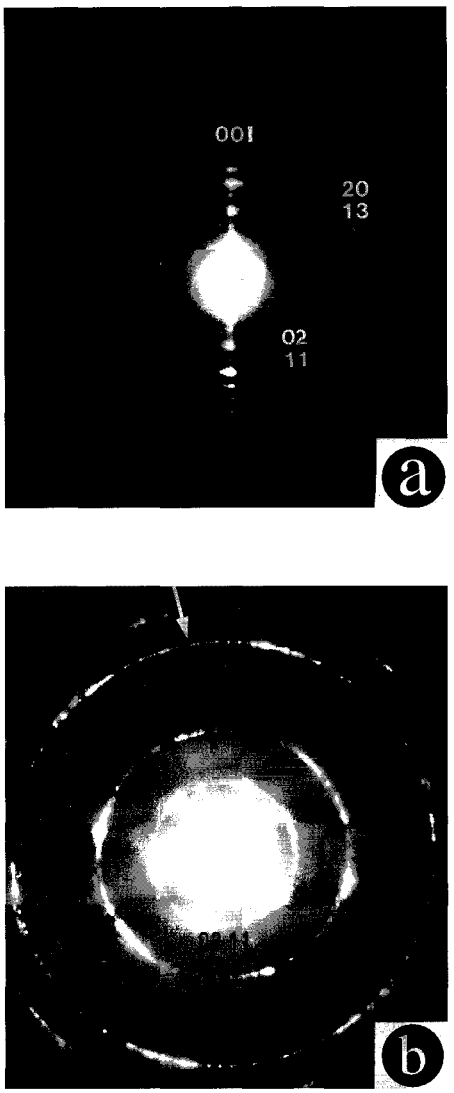

FIGURE 9. SAED patterns of corrensite from sample SC1603. (**a**) Pattern recorded parallel to the layers. (**b**) Pattern recorded normal to the layers; the white arrow points to discrete reflections with unequal intensities, each of which is attributed to small coherent domains poorly extended along c^*.

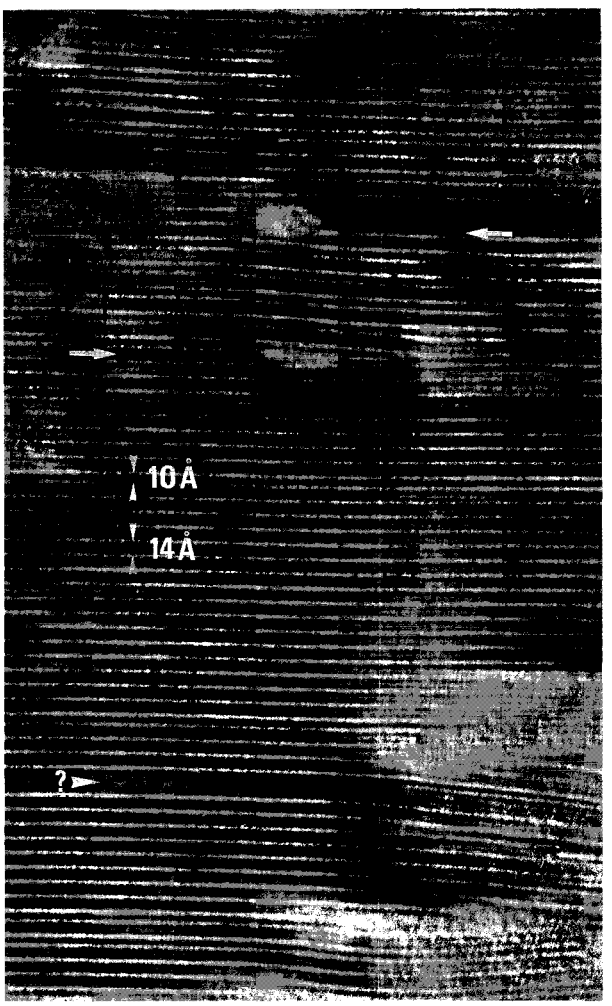

FIGURE 10. Sample SC1379, smectite 25%–chlorite 75%. HRTEM lattice image of the representative chloritic material displaying a flexed, subparallel slab of corrensite (CORR) interlayered with a chlorite matrix (CHL). Here, chlorite (and chlorite-like layers) and smectite-like layers image as 14 and 9–10 Å (collapsed smectite), respectively. Some smectite-like layers are scattered in the chlorite matrix. White arrows point to an extra smectite-like layer (top) and an extra chlorite-like layer (bottom) forming a defect dipole across the corrensite slab. The 28 Å thick layer marked by the white arrow head was not identified.

from crystallites show three types of 00*l* diffraction rows, which occur with similar frequencies: (1) $(14\ \text{Å})^{-1}$ equispaced reflections with intensities typical of trioctahedral Mg-rich chlorite (e.g., 004, 006 ≫ 001, 002, 003, and 005), (2) $(24\ \text{Å})^{-1}$ reflections that are diagnostic of collapsed corrensite (e.g., 001, 002, 003, 005, 007, 0010 > 004, 006, and 009), and (3) superposition of the two former types with some loss of sharpness of reflections along c^*. The corresponding (00*l*) lattice-fringe images of Mg-rich chlorite crystallites exhibit rare and isolated 9–10 Å spaced layers (talc-like or collapsed smectite-like layers?). Corrensite crystallites have the same structural characteristics as sample SC1603. The third type refers to crystallites composed of two regions: one in which corrensite ordering is present and the other with the characteristics of the Mg-rich chlorite described above. In other words, chlorite and corrensite coexist as separate but intergrown phases with very low mutual solubility (very few 9–10 Å layers in chlorite, very few extra 14 Å layers in corrensite). Where finely intergrown, these two types of material produce the third type of SAED pattern that is a superposition of 00*l* reflections of both chlorite and corrensite with streaking along c^* caused by the thin domains of each type piled up along the normal to the layers.

The AEM chemical analysis of SC1379-1 corresponds

to a nearly pure corrensite packet, and the analysis of SC1379-2 corresponds to a packet in which corrensite and chlorite layers are finely intergrown (Fig. 1 and Table 2). The SC1379-1 analysis is similar to the SC1603-1 analysis except that Fe/(Fe + Mg) is much higher (0.37 vs. 0.26). The analysis of SC1379-2 differs from the analysis of nearly pure corrensite by lower Si/(Si + Al) ratio (0.67 vs. 0.71), much lower interlayer charge (0.62 vs. 1.31), and higher octahedral occupancy (18.73 vs. 18.20). These differences are consistent with the increasing proportion of chloritic layers observed in this site. As previously observed for sample SC1603, the Fe/(Fe + Mg) ratios of nearly pure corrensite and material consisting of intergrown corrensite and chlorite do not vary significantly (0.37 and 0.38, respectively). The results of mean microprobe analyses of samples SC1379 and SC1379-2 are similar (Tables 1 and 2). This indicates that, at a larger scale, the intergrowth of corrensite and chlorite predominates in the chloritic material of sample SC1379.

Sample SC961 (chloritic mixed layer with 90% chlorite)

The XRD patterns of sample SC961 (Figs. 5 and 6) are similar to that of true chlorite but differ in the following characteristics: (1) higher intensity of the 001 and relative weakness of the 003 and 004 reflections; (2) presence of a very weak (and broad) superstructure reflection around 29 Å (AD) and 31 Å (EG); (3) weak asymmetry of diffraction peaks occurring near intense corrensite reflections (e.g., 003_{chl},006_{corr} and 004_{chl},008_{corr} reflections in the AD pattern and 001_{chl},002_{corr} and 002_{chl},004_{corr} reflections in the EG pattern), which is characteristic of minor amounts of expandable 2:1 layer silicate.

The actual structure of the expandable 2:1 layer silicate was not determined because of very weak XRD reflections and partial overlap with the tails of stronger neighboring chlorite XRD reflections. The major discrete chlorite peak present in this clay separate represents the major phase and corresponds to poorly crystallized chlorite particles (FWHM = 0.7° 2θ Cu$K\alpha$) that are not consistent with impurities of residual metamorphic chlorite.

The chloritic material does not exhibit a boxwork pattern in SEM images (Fig. 3d). It is composed of coarse packets of small (<1 μm) oriented individual crystals. The basal crystal faces typically present euhedral morphologies. Observed by TEM (Fig. 11) the phyllosilicate material consists of two types of crystallites forming subparallel packets. One type has 14 Å thick layers only, i.e., they are chloritic grains typically 10–40 layers thick. Close observation of the extension of random two-dimensional images indicates that most of the chlorite stacking is coherent with few turbostratic rotations. The second type of crystallite is less common and composed of segregated corrensite and chlorite slabs. Turbostratic stacking is consistently more frequent in corrensite than in chlorite slabs. No separate crystals of corrensite were observed. Such microstructures suggest a rather low structural solubility of corrensite into chlorite.

The results of the AEM chemical analyses of nearly pure chlorite packets of sample SC961 are close to the ideal chlorite composition, in which tetrahedral and octahedral Al contents are equal and the octahedral occupancy is close to 12 cations on the basis 22 O atoms (Fig. 1 and Table 2). These results differ slightly from the microprobe results (Table 1), mostly by showing a lower Si/(Si + Al) ratio (0.60 vs. 0.62) and a higher octahedral occupancy (11.88 vs. 11.66). This clearly shows that microprobe analyses correspond to a local mixture of chlorite and corrensite, as shown above by the HRTEM observations.

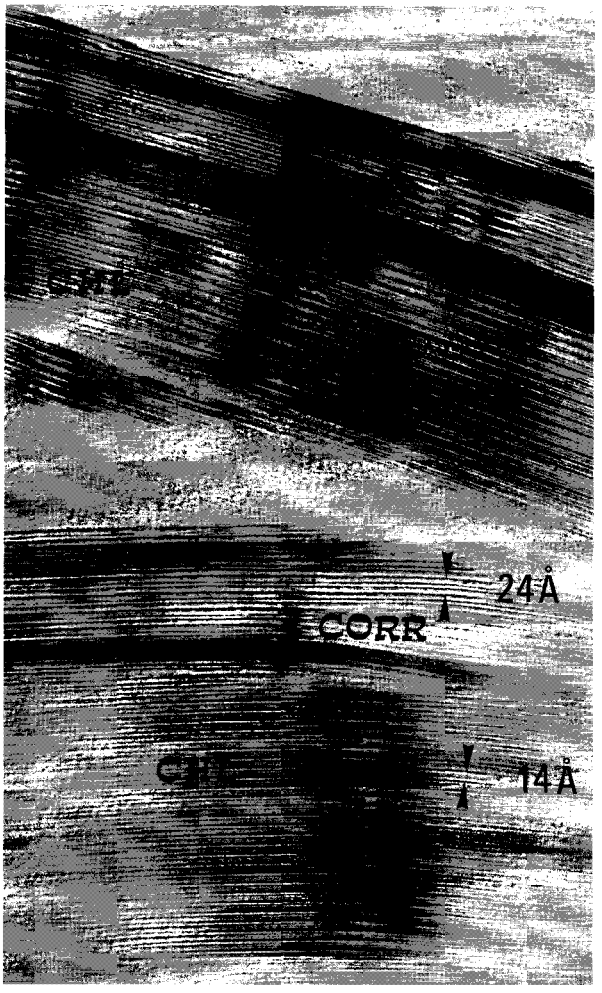

FIGURE 11. Sample SC961, smectite 10%–chlorite 90%. A 00*l* lattice image of representative crystals formed by structurally pure chlorite (CHL) and by the chlorite-corrensite (CHL-CORR) association. The first type largely dominates in the sample, whereas the second type often appears as a corrensite overgrowth on a chlorite core. Corrensite appears preferentially along low-angle grain boundaries.

Decomposition of experimental X-ray diffraction profiles

A decomposition analysis was performed on the XRD profiles. The DECOMPXR routine (Lanson and Besson

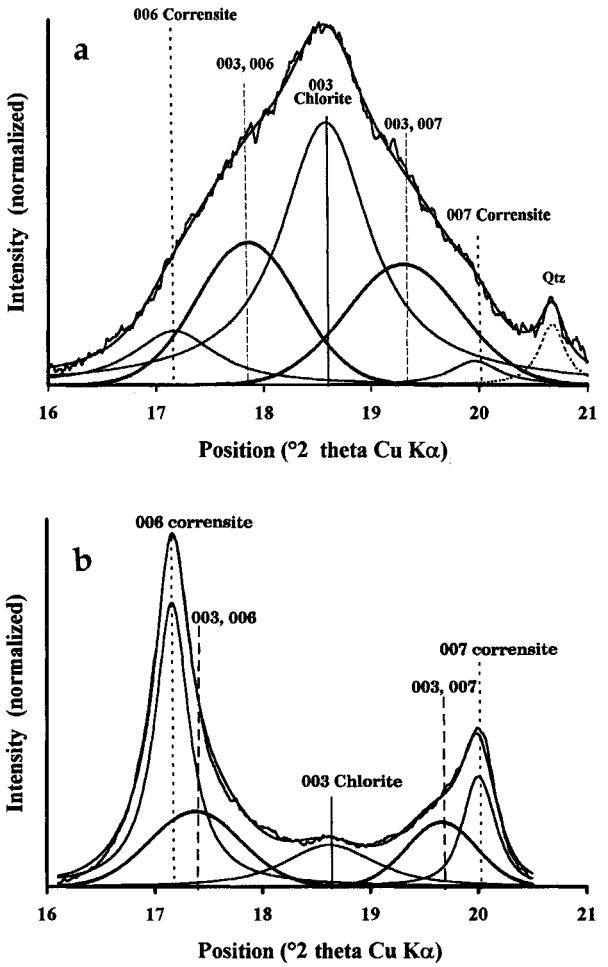

FIGURE 12. Decomposition of the peak near the chlorite 003 position of the EG-solvated samples SC1379 (**a**) and SC1603 (**b**). Dashed lines depict the 006 and 007 peaks of the corrensite diffraction pattern, and solid lines depict the position of the chlorite 003 reflection.

1992; Lanson 1996) permits, even for complex clay assemblages, separation of the various contributions to the diffracted intensity. Any elementary peak can be identified by matching its characteristics (position and width) to those of simulated diffraction peaks. In this study, the decomposition analysis focused on the complex diffraction band near the chlorite 003 peak, which is known to be diagnostic for the identification of C-S mixed layers (Moore and Reynolds 1989). The best fits were obtained with a Lorentzian peak shape for chlorite or corrensite and with a composite of two Gaussian peaks 003_{chl},006_{corr} and 003_{chl},007_{corr} for mixed-layer chlorite-corrensite. The consistency of the decomposition analysis was also verified by comparison with microstructural observations (TEM lattice imaging).

Sample SC1379. The diffraction profile of sample SC1379 is particularly interesting because the peak observed in AD conditions broadens significantly after EG solvation but remains almost symmetrical (Fig. 6). This behavior results from the presence of elementary peaks characteristic of mixed-layer minerals. A close fit of the complex experimental profile may be obtained with five elementary peaks (Fig. 12a). One may be attributed to the 003 peak of chlorite, whereas the discrete corrensite packets observed in TEM are characterized by the 006 and 007 peaks of corrensite. The remaining peaks have intermediate positions between those of chlorite and corrensite. An adequate fit may also be obtained without the discrete corrensite component (with three elementary peaks).

Sample SC1603. The decomposition of the complex diffraction band near the chlorite 003 position of nearly pure corrensite (sample SC1603) shows two weak elementary peaks suggesting minor amounts of C-C mixed layer in addition to the dominant corrensite (Fig. 12b). Peak decomposition of sample SC1603 also reveals a weak and broad peak of discrete chlorite and suggests an incipient separation of very small chlorite crystallites in the corrensitic material.

Sample SC961. Because of the presence of I-S (peak near 5 Å) and amphibole (peak near 4.5 Å) impurities, the decomposition of the pattern for sample SC961 is not discussed; the increased number of adjustable parameters did not permit a unique solution.

Simulation of the X-ray diffraction profiles

Identification of the elementary peaks with positions intermediate between those of chlorite and corrensite (Fig. 12) was performed by comparison with simulated XRD profiles. This comparison was initially performed for the 16–21° 2θ Cu$K\alpha$ range (5.50–4.25 Å). This preliminary identification was then confirmed over the entire 2–30° 2θ Cu$K\alpha$ range (44.0–3.0 Å).

Sample SC1379. The behavior of the 003 diffraction peak after EG solvation is not consistent with a randomly interstratified chlorite-smectite mixed layer. In C-S with R = 0 mixed layer, even for low smectite contents, the peak near the 003 position of chlorite would have marked asymmetry because of a composite 003-003 reflection at slightly lower angular position (Fig. 13). As Hillier (1995) showed, one may always find a mixed-layer C-C (R = 0) equivalent to any C-S (R = 1); the latter were not simulated. Consequently, peaks with positions intermediate between those of chlorite and corrensite were matched to simulated C-C XRD profiles. One should note that not only are the positions of these elementary peaks consistent with a C-C mixed layer but so too is their intensity ratio (i.e., 003_{chl},006_{corr} is more intense than 003_{chl},007_{corr}). This is valid also for the following reflections of the EG sample: 001_{chl},002_{corr}; 002_{chl},003_{corr}; 004_{chl},009_{corr}; and 005_{chl},011_{corr}. However, although the peak positions are compatible, one should note that C-C (R = 1) with a maximum possible degree of ordering (MPDO) induces sharp peaks that should have been resolved during the XRD study. Furthermore, R = 1 with MPDO induces a sharp superstructure peak near 22.5 Å

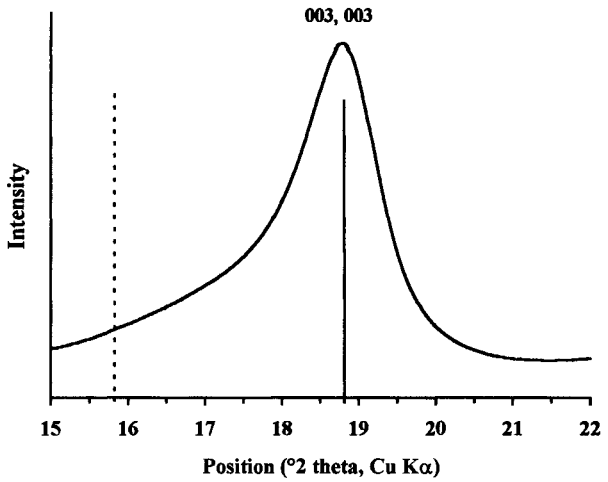

FIGURE 13. NEWMOD simulation of chlorite-smectite (75:25) random mixed layer in the 15–21° 2θ Cu$K\alpha$ range for the following parameters: 25% high-charge (0.60) trioctahedral smectite with two layers of ethylene glycol, d_{001} = 16.9 Å, Fe = 0.4, Ca-exchangeable cation; 75% trioctahedral chlorite, d_{001} = 14.2 Å, Fe = 1.2, Fe in brucite layer = 0, Nbru = 1. 7 < N < 20. The dashed line depicts the peak of the saponite 003 reflection, and the solid line shows the position of the chlorite 003 reflection.

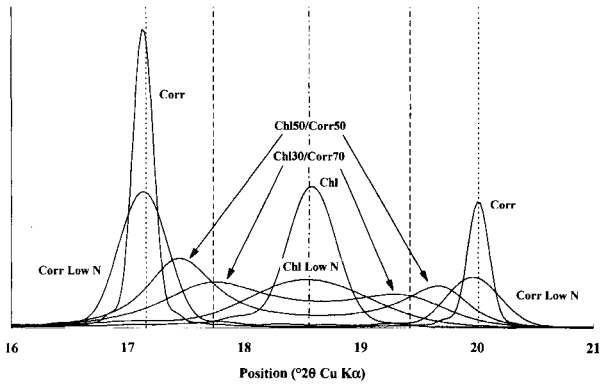

FIGURE 14. Calculated X-ray diffraction patterns of randomly interstratified (R = 0) C-C mixed-layer minerals. Ethylene glycol–solvated corrensite layer: d_{001} = 31.05, $^{[6]}$Fe = 1.0, brucitic Fe = 0.0, exchange capacity = 0.4; chlorite layer: d_{001} = 14.3, $^{[6]}$Fe = 1.4, brucitic Fe = 0.0, brucite layer = 1.0. Coherent-scattering domain size ranges from 5 to 15 layers, except for low-N chlorite and corrensite ($3 \leq N \leq 6$). Dashed lines show the positions of elementary lines associated with corrensite (short dash), C-C mixed layer (long dash), and chlorite (irregular dash).

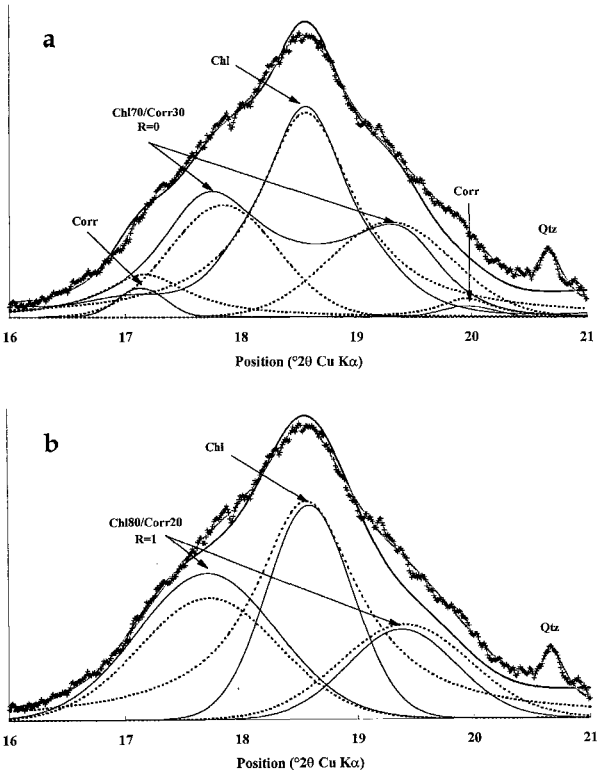

FIGURE 15. Comparison between experimental (EG-solvated sample SC1379 = plus signs) and simulated X-ray patterns in the 16–21° 2θ Cu$K\alpha$ range. (**a**) Dashed lines represent the decomposition of this band in five elementary peaks (see Fig. 12a). Solid lines represent the mixture of calculated (see Fig. 14) chlorite, corrensite, and 70:30 C-C mixed layer (R = 0). A linear background was added both to the mixture of calculated patterns and to the sum of fitted elementary peaks. (**b**) Dashed lines represent the decomposition of this band in three elementary peaks. Solid lines represent a calculated 80:20 C-C mixed layer (R = 1, $P_{corr\text{-}chl}$ = 0.65) and the elementary contributions to this calculated pattern as determined from decomposition. A linear background was added both to the calculated pattern and to the sum of fitted elementary peaks.

that has not been observed in the experimental EG pattern. Thus, R = 1 with MPDO can be rejected as an explanation for the two elementary peaks positioned between those of chlorite and corrensite. No attempt was made to simulate these profiles using the fundamental particle model.

Two alternative nanostructural models give correct simulations. In one of these models, discrete chlorite and corrensite are intergrown with C-C random mixed layers. The simulated position of the two mixed-layer peaks suggests that the chlorite content of this mixed-layer C-C is about 70% (Fig. 14). This appears to be an overestimation of the corrensite abundance with respect to TEM observation of lattice fringes. However, XRD data are presumably more reliable because TEM data may be biased by more selective electron-beam damage of this phase in comparison with that of chlorite. By mixing simulated patterns of chlorite (about 55%), corrensite (about 5%), and a 70:30 C-C mixed layer (about 40%), it is possible to fit the experimental diffraction profile (Fig. 15a).

In the second alternative model, the clay material is essentially composed of an ordered (R = 1) C-C mixed layer with partial segregation. Even though the fit obtained with the above model is good, it is not unique. Hillier (1995) obtained a similar pattern by calculating

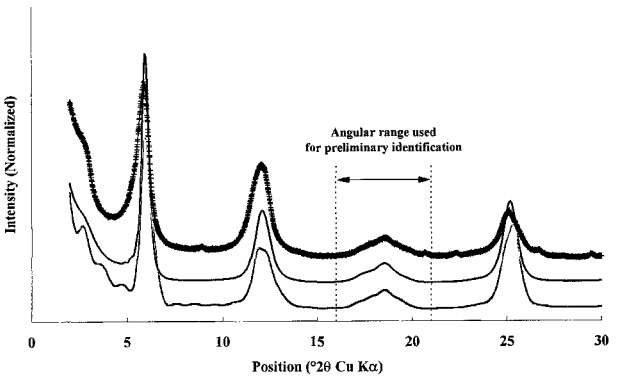

FIGURE 16. Comparison between experimental (EG-solvated sample SC1379, heavy top line) and simulated X-ray patterns in the 2–30° 2θ Cu$K\alpha$ domain. Bottom line represents the mixture of calculated chlorite, corrensite, and R = 0, 70:30 C-C mixed layer (Fig. 15a). Middle line represents a calculated 80:20 C-C mixed layer with R = 1 and $P_{corr\text{-}chl}$ = 0.65 (Fig. 15b). The relative intensities of the diffraction maxima near 12 and 25° 2θ Cu$K\alpha$ were not optimized during the fit.

the XRD profile of an R = 1 C-C mixed layer, assuming partial segregation instead of MPDO. In this case Hillier (1995) showed that the shoulder observed at 31 Å is not related to any ordering but rather to the presence of a 31 Å elementary layer (i.e., corrensite). One must also remember the very low mutual solubility of corrensite and chlorite observed with HRTEM, which argues for a statistical description in terms of segregated mixed layering. An acceptable fit of the 16–21° 2θ Cu$K\alpha$ range (Fig. 15b) was obtained with an 80:20 C-C mixed layer, assuming R = 1 ordering and $P_{corr\text{-}chl}$ = 0.65, which corresponds to an α parameter or proportion of segregation of 18.75% (Lanson 1990).

A comparison of the experimental XRD pattern with the patterns calculated from the two models shows that both simulations roughly work except for the relative intensities of the reflections near the chlorite 002 and 004 peaks, which have not been optimized (Fig. 16). The profile calculated for the C-C ordered mixed layer containing partial segregation fits the experimental pattern slightly better in the low-angle range (2–6° 2θ Cu$K\alpha$).

Sample SC1603. The position of the two mixed-layer peaks in comparison with the position of the 003 peak of chlorite and the positions of the 006 and 007 peaks of corrensite is compatible with random interstratification of chlorite (about 10–20%) and corrensite (Fig. 14).

DISCUSSION

Corrensite: An ordered mixed-layer chlorite-smectite or a discrete phase?

At Sancerre-Couy, saponite, corrensite, and chlorite have been identified in the clay material of the late vein-alteration stage. These trioctahedral phyllosilicates have been widely studied over the last several years with respect to the smectite-to-chlorite conversion, and the debate on the nature of this conversion is still controversial. Two models have been proposed:

The classical model is analogous to that for I-S conversion (Inoue et al. 1988; Lanson and Champion 1991). According to this model, the smectite-to-chlorite conversion proceeds by continuous change of the relative proportions of the two end-members and involves varying types (random and ordered) of mixed layering. In such a model, corrensite is an intermediate form in the saponite-to-chlorite conversion series (Chang et al. 1986; Reynolds 1980) corresponding to a regular mixed layer that is recognized by a rational series of peaks having a coefficient of variability <0.50 (Bailey 1982).

In the second model (Reynolds 1988; Roberson 1988), corrensite itself is considered an end-member that crystallizes directly and should be regarded as a discrete phase. In this model, randomly interstratified C-S mixed layers do not exist, and chloritic mixed layers are considered as a mixture or interstratification of corrensite and chlorite. From XRD and TEM data, Shau et al. (1990) proposed a crystal-chemical model for the corrensite phase that differs from a simple addition of one chlorite and one smectite layer. They demonstrated the presence of C-C mixed layer in metabasalt from northern Taiwan.

More recently, Robinson and Bevins (1994), using XRD studies, including decomposition analysis of 00*l* peaks of chloritic mixed layers from low-grade metabasites (eastern North Greenland), offered support for the C-S mixed-layer model. However, there was poor agreement between the positions of simulated C-S peaks and adjusted elementary maxima.

In the present study, saponite was observed only where corrensite and chlorite are absent. However, traces of corrensite along with major saponite were detected by XRD in two samples not described here. This is confirmed by the chemical data obtained by EMPA and AEM (Fig. 1), which show a dramatic gap between saponite and corrensite and a continuum between corrensite and chlorite.

The results obtained from the clay material from Sancerre-Couy are not consistent with the smectite-to-chlorite conversion model that includes either a continuous (Chang et al. 1986; Robinson and Bevins 1994) or a discontinuous (Inoue et al. 1988; Inoue and Utada 1991) series of chlorite-smectite mixed layers. The following points support the notion that corrensite behaves as a single mineral phase in the samples from Sancerre-Couy. (1) Corrensite is by far the most common trioctahedral clay mineral in the veins from Sancerre-Couy. Locally it forms a homogeneous monomineralic assemblage exhibiting a remarkably coarse grain size (up to several tens of micrometers). (2) The composition of corrensite is constant among samples. AEM data indicate that packets of corrensite from different assemblages (samples SC1603 and SC1379) have a constant Si/(Si + Al) ratio, even where the Fe/(Fe + Mg) ratio differs in response to the compositional change of lithological units (Table 2). (3) Considering the different *b* parameters of smectite and chlorite, the coherent stacking of these two layer types seems

unlikely: The position of the 06,33 reflections (Table 3) indicates that the *b* parameter determined for corrensite SC1603 (9.246 Å) is not the median between *b* parameters measured for saponite and chlorite (samples SC1001 and SC961, respectively), as would be expected from Vegard's Law. It is much higher than that of saponite (9.21 Å) and similar to that of chlorite (9.252 Å). In chloritic mixed layers, the *b* parameter increases with the chlorite content (9.249 and 9.252 Å for samples SC1379 and SC961, respectively). Very similar values have been measured for saponite, corrensite, and chlorite from a smectite-to-chlorite hydrothermal conversion series by Inoue and Utada (1991) in the Kamikita area (Japan). This suggests that the three-dimensional structure of corrensite is not consistent with a 50:50 C-S ordered mixed layer for which the structural parameters should merely correspond to the mean of both phases. (4) HRTEM images clearly indicate that the corrensite layer cannot be divided. Chlorite-like and smectite-like sublayers of corrensite do not behave independently during crystal growth. All the 10 Å layers observed in the corrensitic or chloritic material are linked to chlorite in corrensite layers (24 Å), even in the case of an edge dislocation or layer termination. Moreover, discrete corrensite packets are intimately associated with discrete chlorite packets in all the chloritic material that was previously assumed to be C-S mixed layers. (5) Results from the decomposition and simulation analysis of XRD profiles are consistent with TEM observations. They confirm that C-S mixed layers do not exist and that C-C mixed layers are present in the clay material previously considered to be chloritic C-S. These C-C mixed layers are always associated, in varied proportions, with discrete corrensite.

However, if all the above arguments testify that corrensite behaves as a phase, the occurrence of a regular alternation of layer types contrasts with a stacking mode of layers that is not unique, which would be required theoretically for an ideal structural phase: Turbostratic and coherent stackings are irregularly mixed in otherwise regularly alternating component layers. This raises the question of why the turbostratically rotated corrensite subgrains terminate with the correct chlorite or saponite sublayers in contact. A possible answer would be the existence of growth units or fundamental particles (Nadeau 1984a, 1984b) composed of two 2:1 layers sandwiching a brucite-like interlayer. The semicoherent or random stacking of such units would account for the entire corrensite structure. Smectite-like interlayers would appear at the contact between these units and would be forced to alternate regularly with brucite-like sheets as successive corrensite interlayers. This model could explain both the regular layer stacking and the irregular stacking angles.

Corrensite-to-chlorite conversion

The results obtained in this work, and particularly the TEM and AEM data, are consistent with the work of Shau et al. (1990) and Buatier et al. (1996). These authors described very similar associations of corrensite and chlorite packets and observed C-C mixed layers on the basis of TEM and SAED observations of metabasalt from Taiwan and hydrothermally altered, clastic sediments recovered at ODP site 858, northern Juan de Fuca Ridge. Unfortunately, the XRD patterns for their chloritic material were not provided or were too poorly resolved to allow detailed XRD characterization of these mixed layers.

TABLE 3. Summary of the *d* values of 06,33 reflections of the clay samples from Sancerre-Couy

Sample	$d_{06,33}$ (Å)
SC1001	1.5350
SC1603	1.5410
SC1379	1.5415
SC961	1.5420

Note: The X-ray diagrams are presented in Beaufort and Meunier (1994).

TEM and SAED analyses of samples SC1379 and SC961 also showed packets in which intimately intergrown corrensite and chlorite result in SAED patterns that may be interpreted in terms of interstratification. The decomposition of the XRD patterns of the samples with differing amounts of chlorite and corrensite layers permits investigation of the microcrystalline organization of the chloritic material and hence of the corrensite-to-chlorite conversion process in natural systems.

Even if the distribution of the trioctahedral phyllosilicate crystal subpopulations from Sancerre-Couy is controlled by host-rock chemistry rather than by the thermal paleogradient, the different assemblages determined in this study can be considered as various stages of the saponite-to-chlorite conversion and specifically of the corrensite-to-chlorite conversion. The following occurrences of trioctahedral phyllosilicates were observed: saponite, saponite + minor corrensite (very rare), corrensite + minor C-C mixed layer (10:90) + very minor chlorite, chlorite + C-C mixed layer (70:30) + minor corrensite, chlorite + minor C-C mixed layer (undetermined ratio) + minor corrensite. No C-S mixed layers occurred in such samples.

TEM observations revealed the low solubility between corrensite and chlorite domains. All these results demonstrate that corrensite-to-chlorite conversion proceeds by the growth of chlorite layers that have a strong tendency to segregate and to form discrete chlorite domains in the corrensitic material. C-C mixed layers belong to this conversion process and correspond to limited zones in which both chlorite and corrensite are intimately intergrown. C-C mixed layering is always poorly developed in comparison with discrete chlorite and corrensite (segregated) domains because of the low solubility between chlorite and corrensite. However, the crystallographic structure of the various C-C mixed layers documented in this study cannot be accurately determined because two models permit satisfactory reproduction of the experimental XRD profiles: intergrowths of chlorite and corrensite + randomly interstratified C-C, and intergrowths of chlorite

(and corrensite) + ordered interstratified C-C with segregations.

However, one must keep in mind that the difference between a segregated mixed layer and a mixture of both end-members plus a randomly interstratified mixed layer seems rather conceptual.

Finally, it is suggested that, because corrensite behaves as a true phase and because of the low solubility between corrensite and chlorite layers, the model of mafic silicate conversion from saponite to chlorite strongly differs from the smectite-to-illite conversion series, which has been studied extensively for the last ten years. Intergrowth of discrete corrensite and chlorite domains dominates over mixed layering and a dramatic compositional gap exists between saponite and corrensite. Consequently, C-C mixed layers identified during the corrensite-to-chlorite conversion cannot be considered as interstratified minerals sensu stricto, as is the case for I-S from the smectite-to-illite conversion series encountered in both hydrothermal or diagenetic environments.

Acknowledgments

Financial support for this study was provided by the Programme Géologie Profonde de la France, Sancerre-Couy (GPF). The authors thank Steve Hillier for the use of his modified version of the NEWMOD program, which permits the interstratification of a corrensite layer. Serge Nitsche is thanked for maintenance of the electron microscope at CRMC². The previous version of this paper greatly benefited from the careful and constructive reviews of Bill Carey, George Guthrie, and Robert C. Reynolds.

References cited

April, R.H. (1980) Regularly interstratified chlorite-vermiculite in contact metamorphosed red beds, Newark Group, Connecticut Valley. Clays and Clay Minerals, 28, 1–11.

———(1981a) Clay petrology of the upper Triassic/lower Jurassic terrestrial strata of the Newark Supergroup, Connecticut Valley, U.S.A. Sedimentary Geology, 29, 283–307.

———(1981b) Trioctahedral smectite and interstratified chlorite-smectite in Jurassic strata of the Connecticut Valley. Clays and Clay Minerals, 29, 31–39.

Bailey, S.W. (1982) Nomenclature for regular interstratifications. American Mineralogist, 67, 394–398.

Baronnet, A., Nitsche, S., and Kang, Z.C. (1993) Layer stacking microstructures in a biotite single crystal: A combined HREM-AEM study. Phase Transitions, 43, 107–128.

Beaufort, D., and Meunier, A. (1983) A petrographic study of phyllic alteration superimposed on potassic alteration: The Sibert porphyry deposit (Rhône, France). Economic Geology, 78, 1514–1527.

Beaufort, D., Meunier, A., Thomassin, J.H., and Fouillac, A.M. (1991) Corrensite, chlorite-smectite mixed-layered minerals and saponite in the metamorphic basement of the Basin of Paris (France). In Proceedings of 7th Euroclay Conference, Dresden, 1, 65–69.

Beaufort, D., and Meunier, A. (1994) Saponite, corrensite and chlorite/saponite mixed-layered minerals and saponite in the Sancerre-Couy deep drill hole (France). Clay Minerals, 29, 47–61.

Bettison, L.A., and Schiffman, P. (1988) Compositional and structural variations of phyllosilicate from the Point Sal ophiolite, California. American Mineralogist, 73, 62–76.

Bodine, M.W., and Madsen, B.M. (1987) Mixed-layer chlorite-smectites from a Pennsylvanian evaporite cycle, Grand Country, Utah. In L.G. Schultz, H. van Holphen, and F.A. Mumpton, Eds., Proceedings of the International Clay Conference, Denver, 1985, p. 85–93. Clay Minerals Society, Bloomington, Indiana.

Boulègue, J., Benedetti, M., Gautier, B., and Bosch, B. (1990) Les fluides dans le socle du sondage GPF Sancerre-Couy. Bulletin de la Société Géologique de France, 8, 789–795.

Boulègue, J., and Mégnien, C. (1992) Forage scientifique de Sancerre-Couy: Les fluides libres du socle. Géologie de la France, 3–4, 157–166.

Buatier, M., Früh-Green, G.L., and Karpoff, A.M. (1996) Mechanisms of Mg-phyllosilicates formation in a hydrothermal system at a sedimented ridge (Middle Valley, Juan de Fuca). Contributions to Mineralogy and Petrology, 122, 134–151.

Chang, H.K., Mackenzie, F.T., and Schoonmaker, J. (1986) Comparison between the diagenesis of dioctahedral and trioctahedral smectite, Brasilian offshore basins. Clays and Clay Minerals, 34, 407–423.

Cliff, G., and Lorimer, G.W. (1975) The quantitative analysis of thin specimens. Journal of Microscopy, 103, 203–207.

Fouillac, A.M., and Beaufort, D. (1991) Etude minéralogique et isotopique (^{13}C, ^{18}O) des carbonates néoformés dans le sondage profond de Sancerre-Couy (France). Bulletin de la Société Géologique de France, 162, 939–945.

———(1992) A stable isotope study of clay minerals from the Sancerre Couy deep drill hole, Paris Basin (France). Proceedings of the 7th Water-Rock Interaction, Park City, Utah, V2, 1227–1229.

Guthrie, G.D., Jr., and Veblen, D.R. (1990) Interpreting one-dimensional high-resolution transmission electron micrographs of sheet silicates by computer simulation. American Mineralogist, 75, 276–288.

Hillier, S. (1995) Mafic phyllosilicates in low-grade metabasites: Characterization using deconvolution analysis—Discussion. Clay Minerals, 30, 67–73.

Hoffman, J., and Hower, J. (1979) Clay minerals assemblages as low grade metamorphic geothermometers: Application to the thrust fault disturbed belt of Montana, U.S.A. In Aspects of Diagenesis, SEPM Special Publications, 26, 55–79.

Inoue, A. (1987) Conversion of smectite to chlorite by hydrothermal diagenetic alterations, Hokuroku Kuroko mineralization area, Northeast Japan. In L.G. Schultz, H. van Olphen, and F.A. Mumpton, Eds., Proceedings of the International Clay Conference, Denver, 1985, p. 158–164. Clay Minerals Society, Bloomington, Indiana.

Inoue, A., Velde, B., Meunier, A., and Touchard, G. (1988) Mechanism of illite formation during smectite-to-illite conversion in a hydrothermal system. American Mineralogist, 73, 1325–1334.

Inoue, A., and Utada, M. (1991) Smectite-to-chlorite transformation in thermally metamorphosed volcanoclastic rocks in the Kamikita area, northern Honshu, Japan. American Mineralogist, 76, 628–640.

Johnson, L.J. (1964) Occurrence of regularly interstratified chlorite-vermiculite as a weathering product of chlorite in a soil. American Mineralogist, 49, 556–572.

Klimentidis, R.E., and Mackinnon, D.R. (1986) High resolution imaging of ordered mixed-layer clays. Clays and Clay Minerals, 34, 155–164.

Kristmannsdottir, H. (1979) Alteration of basaltic rocks by hydrothermal activity at 100–300 °C. In M.M. Mortland and V.C. Farmer, Eds., Proceedings of the 6th International Clay Conference, p. 359–367, Elsevier, Amsterdam.

Lanson, B. (1990) Mise en évidence des mécanismes de transformation des interstratifiés illite/smectite au cours de la diagenèse, 366 p. Ph.D. thesis, University Paris, France.

———(1996) Decomposition of experimental X-ray diffraction patterns (profile fitting): A convenient way to study clay minerals. Clays and Clay Minerals, in press.

Lanson, B., and Champion, D. (1991) The I-S to illite reaction in the late stage diagenesis. American Journal of Science, 291, 473–506.

Lanson, B., and Besson, G. (1992) Characterization of the end of smectite-to-illite transformation: Decomposition of X-ray patterns. Clays and Clay Minerals, 40, 40–52.

Lippmann, F. (1956) Clay minerals from the Röt member of the Triassic near Göttingen, Germany. Journal of Sedimentary Petrology, 26, 125–139.

Meunier, A., Inoue, A., and Beaufort, D. (1991) Chemographic analysis of trioctahedral smectite-to-chlorite conversion series from the Ohyu Caldera, Japan. Clays and Clay Minerals, 39, 409–415.

Moore, D.M., and Reynolds, R.C. (1989) Identification of mixed-layered clay minerals. In D.M. Moore and R.C Reynolds, Eds., X-ray diffrac-

tion and the identification and analyses of clay minerals, p. 241–269. Oxford University Press, U.K.

Nadeau, P.H., Tait, J.M., Mc Hardy, W.J., and Wilson, M.J. (1984a) Interstratified XRD characteristics of physical mixtures of elementary clay particles. Clay Minerals, 19, 67–76.

Nadeau, P.H., Wilson, M.J., Mc Hardy, W.J., and Tait, J.M. (1984b) Interparticle diffraction: A new concept for interstratified clays. Clay Minerals, 19, 757–769.

Post, J.L., and Janke, N.C. (1974) Properties of "swelling" chlorites in some mesozoic formations of California. Clays and Clay Minerals, 22, 67–76.

Reynolds, R.C. (1980) Interstratified clay minerals. In G.W. Brindley and G. Brown, Eds., Crystal structures of the clay minerals and their X-ray identification, p. 249–303. Mineralogical Society, London, U.K.

——— (1985) NEWMOD, a computer program for the calculation of one-dimensional diffraction patterns for mixed-layered clays. R.C. Reynolds, Hanover, New Hampshire.

——— (1988) Mixed-layer chlorite minerals. In Mineralogical Society of America Reviews in Mineralogy, 19, 601–609.

Roberson, H.E. (1988) Random mixed-layer chlorite-smectite: Does it exist? (abs.). Clay Minerals Society, 25th Annual General Meeting.

Robinson, D., and Bevins, R.E. (1994) Mafic phyllosilicates in low-grade metabasites: Characterization using deconvolution analysis. Clay Minerals, 29, 223–237.

Schultz, L.G. (1963) Clay minerals in the Triassic rocks of the Colorado Plateau. U.S. Geological Survey Bulletin, 1147-C, 1–71.

Shau, Y.H., Peacor, D.R., and Essene, E.J. (1990) Corrensite and mixed-layer chlorite/corrensite in metabasalts from northern Taiwan: TEM/AEM, EMPA, XRD and optical studies. Contributions to Mineralogy and Petrology, 105, 123–142.

Vali, H., and Koster, H.M. (1986) Expanding behaviour, structural disorder, regular and random irregular interstratification of 2:1 layer-silicates studied by high-resolution images of transmission electron microscopy. Clay Minerals, 21, 827–859.

Velde, B. (1977) Clays and clay minerals in natural and synthetic systems, 218 p. Elsevier, Amsterdam.

Vergo, N., and April, R.H. (1982) Interstratified clay minerals in contact aureoles, West Rock, Connecticut. Clays and Clay Minerals, 30, 237–240.

Whitney, G., and Northrop, H.R. (1986) Vanadium chlorite from a sandstone host vanadium-uranium deposit, Henry Basin, Utah. Clays and Clay Minerals, 34, 488–495.

MANUSCRIPT RECEIVED OCTOBER 16, 1995
MANUSCRIPT ACCEPTED SEPTEMBER 16, 1996